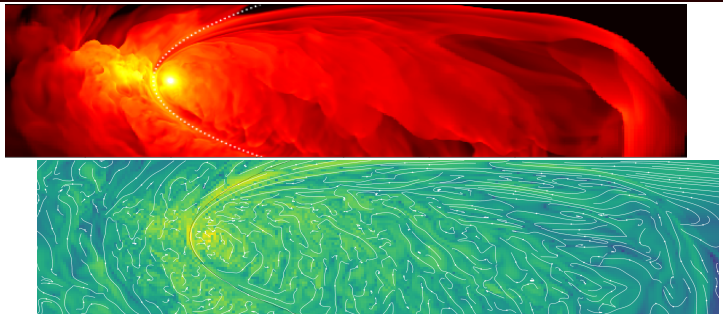

Tidal disruption of a magnetized star

ApJ 1001, 71; arXiv:2509.23894

Pavel Abolmasov, Omer Bromberg, Amir Levinson, Ehud Nakar

The Raymond and Beverly Sackler School of Physics and Astronomy, Tel Aviv University,
Simons Collaboration on Extreme Electrodynamics of Compact Sources

TDE prediction

- The idea of tidal disruption (Hills1975; Lidskii & Ozernoi1979)
- Conventional picture (Rees1988; Evans & Kochanek1989)
- Distribution in energy and fallback rate power law $\dot{M} \propto t^{-5/3}$ (Evans & Kochanek1989)

Tidal radius:

$$R_{\rm t} \simeq R_* \left(\frac{M_{\rm BH}}{M_*}\right)^{1/3}$$

Penetration parameter:

$$\beta = \frac{R_{\rm t}}{R_{\rm p}}$$

Elliptic orbits with

$$a \gtrsim \frac{R_{\rm t}^2}{R_*} \sim R_* \left(\frac{M_{\rm BH}}{M_*}\right)^{2/3}.$$

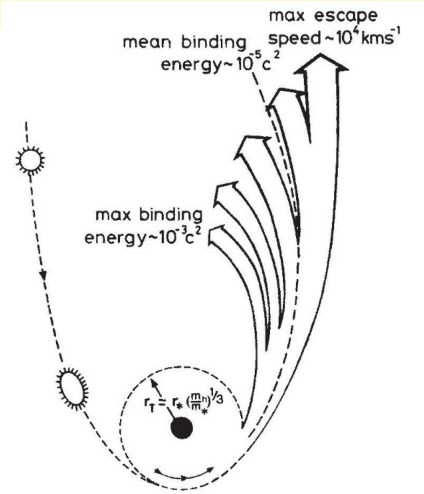

from Rees1988)

TDE prediction

- The idea of tidal disruption (Hills1975; Lidskii & Ozernoi1979)
- Conventional picture (Rees1988; Evans & Kochanek1989)
- Distribution in energy and fallback rate power law $\dot{M} \propto t^{-5/3}$ (Evans & Kochanek1989)

Tidal radius:

$$R_{\rm t} \simeq R_* \left(\frac{M_{\rm BH}}{M_*}\right)^{1/3}$$

Penetration parameter:

$$\beta = \frac{R_{\rm t}}{R_{\rm p}}$$

Elliptic orbits with

$$a \gtrsim \frac{R_{\rm t}^2}{R_*} \sim R_* \left(\frac{M_{\rm BH}}{M_*}\right)^{2/3}.$$

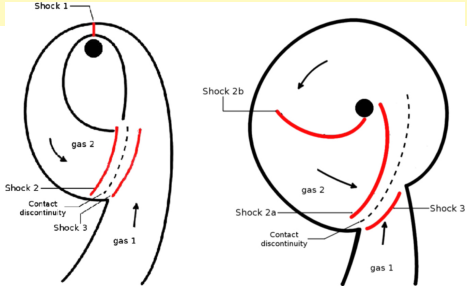

Piran et al.2015)

Relativistic apsidal motion important for large $M_{\rm BH}$, single-orbit angle (see for instance Dai et al.2015)

$$\Delta\varphi \simeq \frac{3\pi G M_{\rm BH}}{R_{\rm p} c^2}. \quad (1)$$

TDE prediction

- The idea of tidal disruption (Hills1975; Lidskii & Ozernoi1979)
- Conventional picture (Rees1988; Evans & Kochanek1989)
- Distribution in energy and fallback rate power law $\dot{M} \propto t^{-5/3}$ (Evans & Kochanek1989)

Tidal radius:

$$R_{\rm t} \simeq R_* \left(\frac{M_{\rm BH}}{M_*}\right)^{1/3}$$

Penetration parameter:

$$\beta = \frac{R_{\rm t}}{R_{\rm p}}$$

Elliptic orbits with

$$a \gtrsim \frac{R_{\rm t}^2}{R_*} \sim R_* \left(\frac{M_{\rm BH}}{M_*}\right)^{2/3}.$$

Time scales: Fly-by time $\sim$ stellar dynamical time

$$t_* \sim t_{\rm ff}(R_{\rm t}) \simeq 2\pi\sqrt{\frac{R_{\rm t}^3}{GM_{\rm BH}}} = 2\pi\sqrt{\frac{R_*^3}{GM_*}} \simeq 50 \left(\frac{R_*}{10\ {\rm R}_\odot}\right)^{3/2} \left(\frac{M_*}{3\ {\rm M}_\odot}\right)^{-1/2} {\rm h}$$

Fallback time

$$t_{\rm fb} \sim \pi\sqrt{\frac{a_{\rm min}^3}{GM_{\rm BH}}} = \frac{1}{2}\sqrt{\frac{M_{\rm BH}}{M_*}}\, t^* \sim \text{months-years.}$$

Energy budget (maximal efficiency):

$$E_{\rm g} \sim \overbrace{\frac{GM_*M_{\rm BH}}{R_{\rm p}}}^{\sim 10^{52}{\rm erg}} \sim \underbrace{\frac{GM_*^2}{R_*}}_{\sim 10^{48}{\rm erg}} \left(\frac{M_{\rm BH}}{M_*}\right)^{2/3}$$

TDE prediction

- The idea of tidal disruption (Hills1975; Lidskii & Ozernoi1979)
- Conventional picture (Rees1988; Evans & Kochanek1989)
- Distribution in energy and fallback rate power law $\dot{M} \propto t^{-5/3}$ (Evans & Kochanek1989)

Tidal radius:

$$R_{\rm t} \simeq R_* \left(\frac{M_{\rm BH}}{M_*} \right)^{1/3}$$

Penetration parameter:

$$\beta = \frac{R_{\rm t}}{R_{\rm p}}$$

Elliptic orbits with

$$a \gtrsim \frac{R_{\rm t}^2}{R_*} \sim R_* \left(\frac{M_{\rm BH}}{M_*} \right)^{2/3}.$$

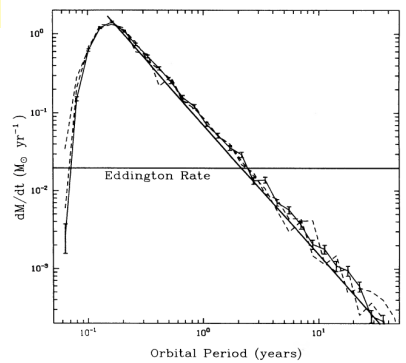

FIG. 4.—The rate at which stellar debris returns to the vicinity of the black hole vs. time. The Eddington accretion rate for a $M_{\rm h} = 10^6\ M_\odot$ black hole, with radiative efficiency $\epsilon = 0.1$, is indicated. The heavy line shows the estimated infall rate given by eq. (3) in the text. The results from three different SPH simulations are shown, with particle resolutions of 10^4, 2×10^4, and 4×10^4 particles per star. The error bars show the level of statistical fluctuations due to binning the particles.

$$\dot{M}_{\rm fallback} \propto t^{-5/3}$$

TDE observations

X-ray nuclear transients and optical/UV transients (50+ in total)

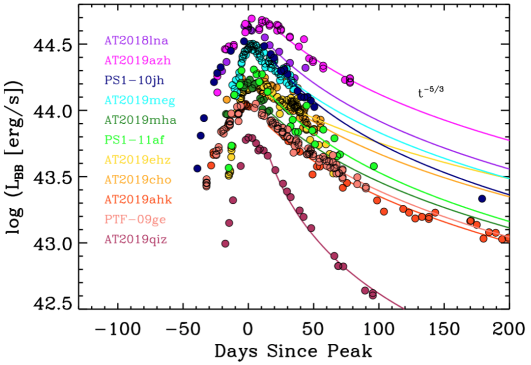

Gezari2021)

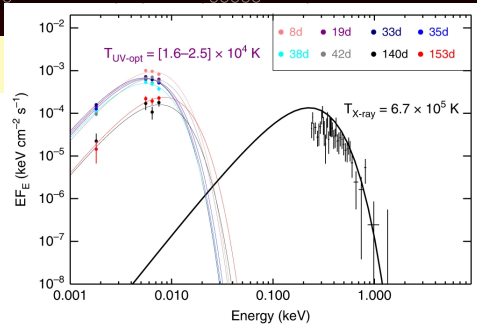

Shu et al.2020)

UV-radiating area $A_{\rm UV} \sim 10^{31} L_{44}^{1/2} (T/2\times10^4{\rm K})^{-2}{\rm cm}^2$,

$A_{\rm X} \sim 10^{24} L_{44}^{1/2} T_6^{-2}{\rm cm}^2$.

Compare to $\pi R_{\rm p}^2 \sim 10^{26} (R_*/\,{\rm R}_\odot)^2 \left({\rm M_{BH}}/10^6{\rm M}_*\right)^{2/3}\,{\rm cm}^2$.

Area within the most bound orbit $\sim 10^{24}\left(M_{\rm BH}/10^6 M_*\right)^2\,{\rm cm}^2$.

Fallback stream area

$\lesssim \pi a^2 \sim 10^{30} (R_*/\,{\rm R}_\odot)^2 \left({\rm M_{BH}}/10^6{\rm M}_*\right)^{4/3}\,{\rm cm}^2$

TDE observations

X-ray nuclear transients and optical/UV transients (50+ in total)

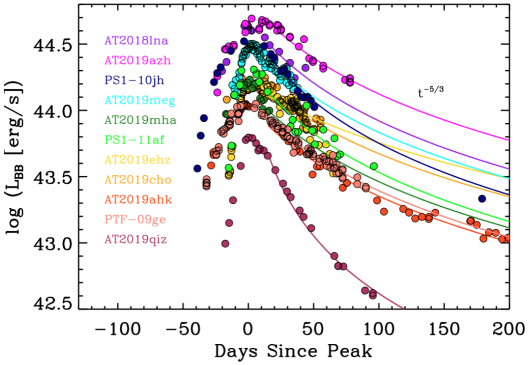

Gezari2021)

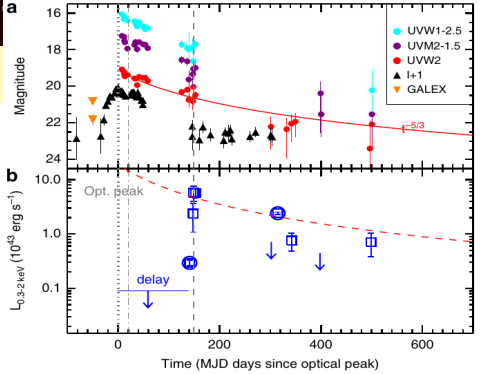

Shu et al.2020)

UV-radiating area $A_{\rm UV} \sim 10^{31} L_{44}^{1/2} (T/2\times10^4{\rm K})^{-2}{\rm cm}^2$,

$A_{\rm X} \sim 10^{24} L_{44}^{1/2} T_6^{-2}{\rm cm}^2$.

Compare to $\pi R_{\rm p}^2 \sim 10^{26} (R_*/\,{\rm R}_\odot)^2 \left({\rm M_{BH}}/10^6{\rm M}_*\right)^{2/3}\,{\rm cm}^2$.

Area within the most bound orbit $\sim 10^{24} \left(M_{\rm BH}/10^6 M_*\right)^2\,{\rm cm}^2$.

Fallback stream area

$\lesssim \pi a^2 \sim 10^{30} (R_*/\,{\rm R}_\odot)^2 \left({\rm M_{BH}}/10^6{\rm M}_*\right)^{4/3}\,{\rm cm}^2$

Radio and jets

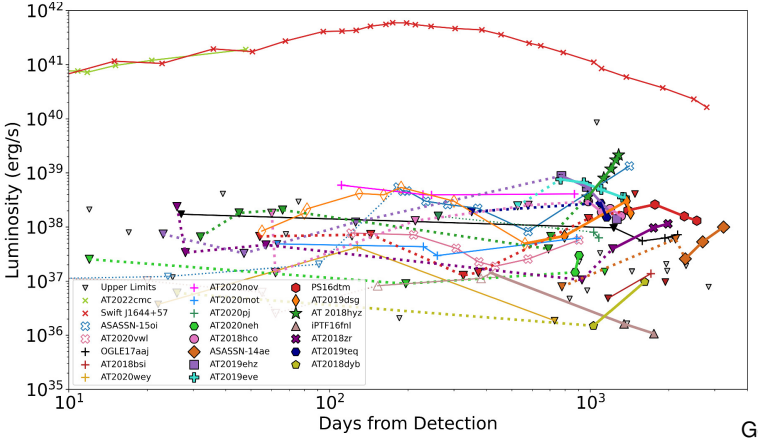

Cendes et al.2024)

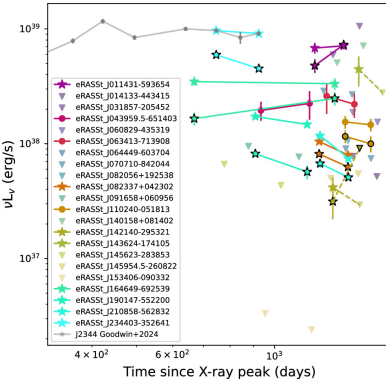

Goodwin et al.2025)

TDE observations: polarization

AT2020mot ⇒

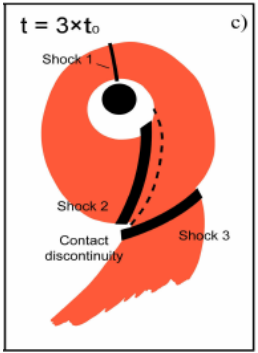

Liodakis et al.2023)

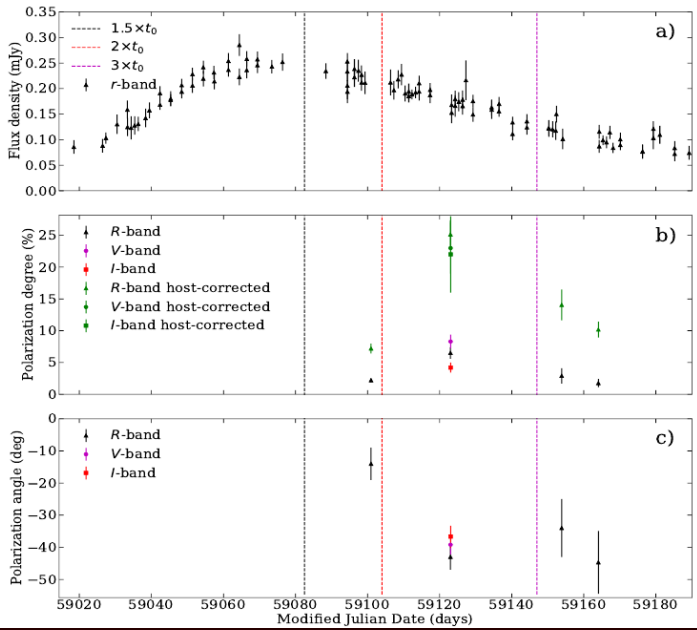

TDE simulations: early stages

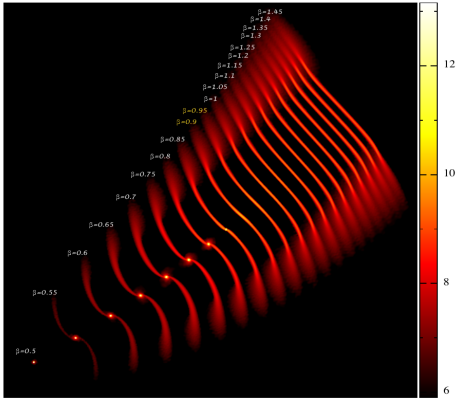

Mainetti et al.2017)

- Smooth Particle Hydrodynamics (SPH)
- star-frame mesh-based hydrodynamics

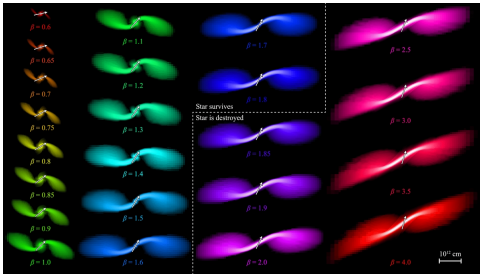

Guillochon & Ramirez-Ruiz2013)

TDE simulations: circularization

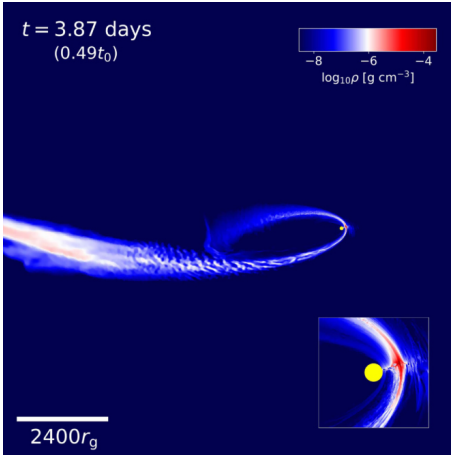

Ryu et al.2023)

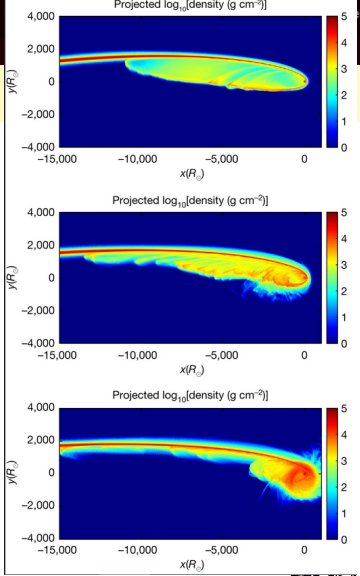

Steinberg & Stone2024)

Pavel Abolmasov, Omer Bromberg, Amir Levinson, Ehud Nakar TAU/SCEECS

Disruption of magnetized stars

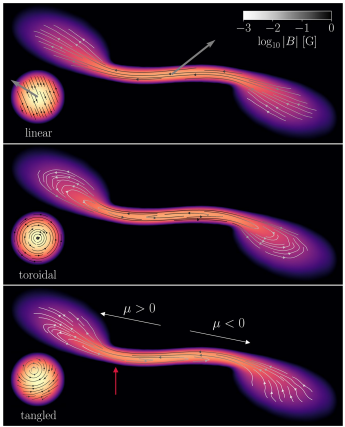

Pacuraru et al.2026)

Magnetic energy of a star

$$\sim E_{\rm M}/E_{\rm G} \sim \frac{B^2 R_*^4}{G M_*^2} \sim 10^{-16} \left(\frac{B}{\rm G}\right)^2 \left(\frac{R_*}{\rm R_\odot}\right)^4 \left(\frac{\rm M_\odot}{M_*}\right)^2 .$$

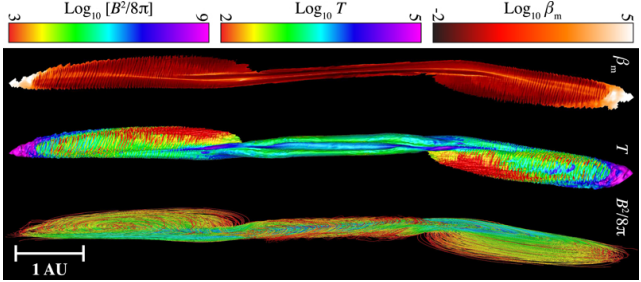

Guillochon & McCourt2017)

The role of magnetic fields:

- disc formation and angular momentum transfer
- jets
- emission mechanisms

The idea of the project:

- MHD grid-based simulation of a magnetized star,
- from the initial frozen-in field towards the fields inside the accretion disc

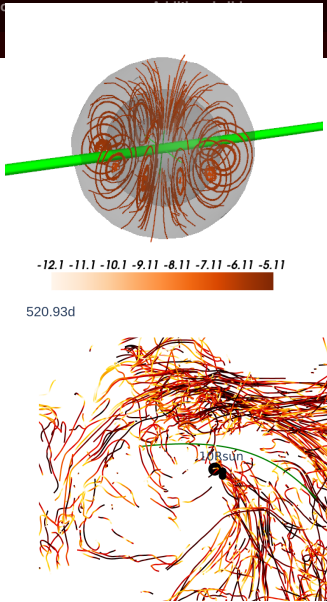

Scales and requirements

- $M_{\rm BH} \sim 10^3..10^6\ {\rm M}_\odot$
- $M_* \sim {\rm M}_\odot$
- $R_* \sim R_\odot$
- tidal disruption radius $R_{\rm t} \sim (M_{\rm BH}/M_*)^{1/3} R_* \sim 100 R_\odot$
- pericenter radius $R_{\rm p}$ and penetration parameter $\beta = R_{\rm t}/R_{\rm p} \gtrsim 1$
- $R_{\rm a} \sim R_{\rm p}^2/R_* \sim (M_{\rm BH}/M_*)^{2/3} R_*/\beta^2 \sim 10^4\ {\rm R}_\odot$
- internal temperature of the star $kT_* \sim GM_*/R_*$
- Mach number of the orbital motion $\mathcal{M} \sim \sqrt{\beta}\,(M_{\rm BH}/M_*)^{1/3} \gtrsim 100$
- density contrast $\rho_*/\rho_{\rm ISM} \gtrsim 10^{-10}$ (maybe a lot more)
- magnetic $\beta \sim 10^{10}$ (?)

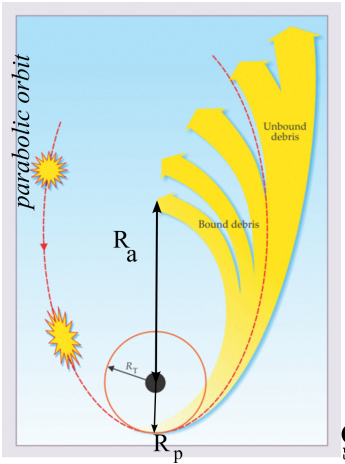

Simulation setup

- `Athena++` non-relativistic ideal MHD, EOS $\gamma = 5/3$
  `https://github.com/pabolmasov/athena-remap.git`
- AMR 4 levels (16 times different resolution)
- star-centred frame, then BH frame
- initial star $R_* = 10\ \mathrm{R}_\odot$ hydrostatic $n = 5$ polytrope, $M = 3\ \mathrm{M}_\odot$
- BH mass $M = 3 \times 10^3\ \mathrm{M}_\odot$ ($\Rightarrow R_\mathrm{G} \simeq 0.01\ \mathrm{R}_\odot$)
- "dipolar" field, $R_1 = 2\ \mathrm{R}_\odot$, $R_2 = 8\ \mathrm{R}_\odot$, minimal plasma $\beta_\mathrm{m} = 10^3$

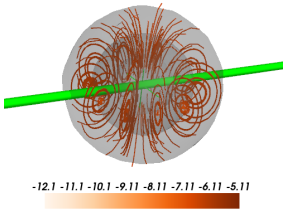

ID	t range, d	frame	limits, $\mathrm{R}_\odot$	resolution $\mathrm{R}_\odot$	self-gravity	mass boost	comment
`S400`	$-1.8..1.0$	star	$400 \times 400 \times 400$	0.2..2	✓	1	disruption stage
`S1000`	0.5..12	star	$2000 \times 2000 \times 2000$	1..8	✓	1	debris expansion
`BH1`	10..30	BH	$-1000..5000$ $\times -3000..1000$ $\times -125..125$	4..16	–	10^3	fallback formation
`BH2`	30..550	BH	$-1000..5000$ $\times -3000..1000$ $\times -600..600$	2.3..18	–	10^3	fallback ($t \sim 40 - 250$d) abalone ($t \sim 60 - 300$d) circularization ($t \sim 300$)
`BHz`	480..550	BH	–	1.2..18	–	10^3	disc zoom-in

Simulation setup

- `Athena++` non-relativistic ideal MHD, EOS $\gamma = 5/3$
  `https://github.com/pabolmasov/athena-remap.git`
- AMR 4 levels (16 times different resolution)
- star-centred frame, then BH frame
- initial star $R_* = 10\ \mathrm{R}_\odot$ hydrostatic $n = 5$ polytrope, $M = 3\ \mathrm{M}_\odot$
- BH mass $M = 3 \times 10^3\ \mathrm{M}_\odot$ ($\Rightarrow R_\mathrm{G} \simeq 0.01\ \mathrm{R}_\odot$)
- "dipolar" field, $R_1 = 2\ \mathrm{R}_\odot$, $R_2 = 8\ \mathrm{R}_\odot$, minimal plasma $\beta_\mathrm{m} = 10^3$

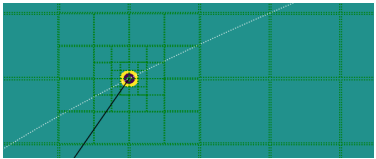

$$A_\varphi = \frac{\sin\theta}{2\pi R}\,(R_2 - R)\,(R - R_1)\,,$$

ID	t range, d	frame	limits, $\mathrm{R}_\odot$	resolution $\mathrm{R}_\odot$	self-gravity	mass boost	comment
`S400`	$-1.8..1.0$	star	$400 \times 400 \times 400$	$0.2..2$	✓	1	disruption stage
`S1000`	$0.5..12$	star	$2000 \times 2000 \times 2000$	$1..8$	✓	1	debris expansion
`BH1`	$10..30$	BH	$-1000..5000$ $\times -3000..1000$ $\times -125..125$	$4..16$	–	10^3	fallback formation
`BH2`	$30..550$	BH	$-1000..5000$ $\times -3000..1000$ $\times -600..600$	$2.3..18$	–	10^3	fallback ($t \sim 40 - 250$d) abalone ($t \sim 60 - 300$d) circularization ($t \sim 300 - 500$d)
`BHz`	$480..550$	BH	–	$1.2..18$	–	10^3	disc zoom-in

Simulation setup

- `Athena++` non-relativistic ideal MHD, EOS $\gamma = 5/3$
  `https://github.com/pabolmasov/athena-remap.git`
- AMR 4 levels (16 times different resolution)
- star-centred frame, then BH frame
- initial star $R_* = 10\ \mathrm{R}_\odot$ hydrostatic $n = 5$ polytrope, $M = 3\ \mathrm{M}_\odot$
- BH mass $M = 3 \times 10^3\ \mathrm{M}_\odot$ ($\Rightarrow R_\mathrm{G} \simeq 0.01\ \mathrm{R}_\odot$)
- "dipolar" field, $R_1 = 2\ \mathrm{R}_\odot$, $R_2 = 8\ \mathrm{R}_\odot$, minimal plasma $\beta_\mathrm{m} = 10^3$

Black hole gravity (pseudo-Newtonian outside $r_0 = 10\ \mathrm{R}_\odot$)

$$g(R) = \begin{cases} \dfrac{GM_\mathrm{BH}}{r^2}\left(\dfrac{1-\frac{2GM}{r_0c^2}}{1-\frac{2GM}{rc^2}}\right)^2 & r > r_0 \\ \dfrac{GM_\mathrm{BH}}{r_0^2}\dfrac{r}{r_0} & r < r_0, \end{cases}$$

ID	t range, d	frame	limits, $\mathrm{R}_\odot$	resolution $\mathrm{R}_\odot$	self-gravity	mass boost	comment
`S400`	$-1.8..1.0$	star	$400 \times 400 \times 400$	0.2..2	✓	1	disruption stage
`S1000`	0.5..12	star	$2000 \times 2000 \times 2000$	1..8	✓	1	debris expansion
`BH1`	10..30	BH	$-1000..5000$ $\times -3000..1000$ $\times -125..125$	4..16	–	10^3	fallback formation
`BH2`	30..550	BH	$-1000..5000$ $\times -3000..1000$ $\times -600..600$	2.3..18	–	10^3	fallback ($t \sim 40 - 250$d) abalone ($t \sim 60 - 300$d) circularization ($t \sim 300 - 500$d)
`BHz`	480..550	BH	–	1.2..18	–	10^3	disc zoom-in

Remapping sequence

1. First simulation 400^3 $R_\odot$, star-centred: disruption up to considerable deformation
2. Remapping to 2000^3 $R_\odot$: up to minimal apocentre distance
3. Switching to the BH frame, self-gravity turned off: up to disc formation

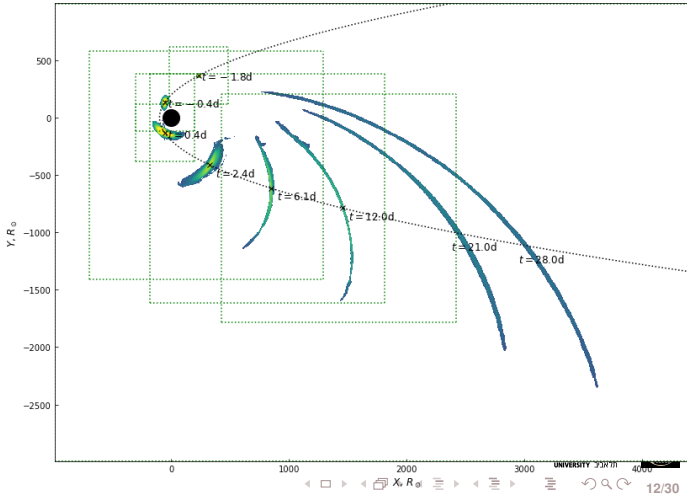

Early magnetic field evolution

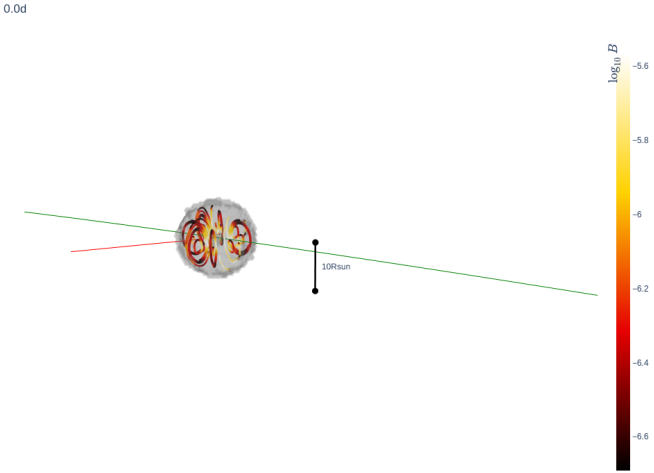

Early magnetic field evolution

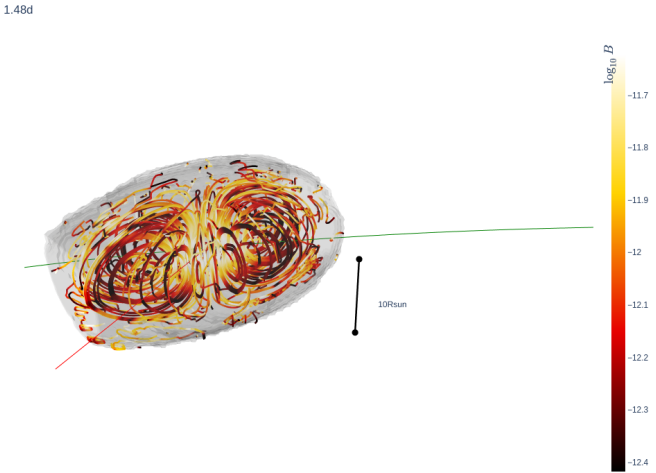

Pavel Abolmasov, Omer Bromberg, Amir Levinson, Ehud Nakar TAU/SCEECS

Early magnetic field evolution

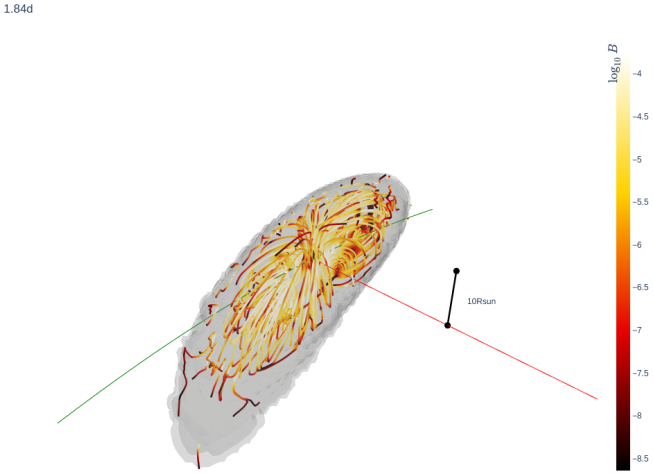

Pavel Abolmasov, Omer Bromberg, Amir Levinson, Ehud Nakar TAU/SCEECS

Early magnetic field evolution

$t = 4.06$

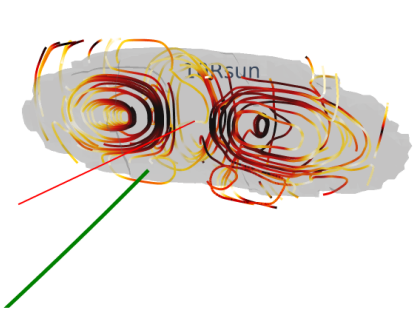

$t = 4.06$

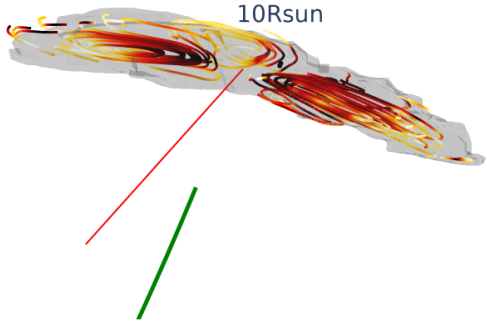

'pancakes' (cf Coughlin et al.2016)

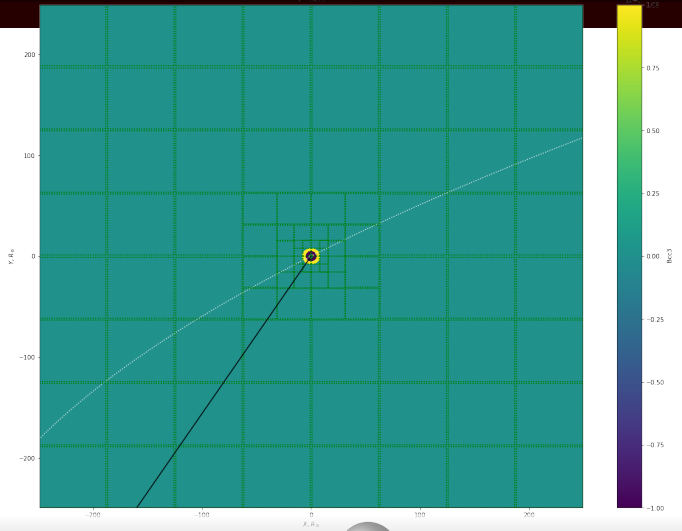

Pavel Abolmasov, Omer Bromberg, Amir Levinson, Ehud Nakar TAU/SCEECS

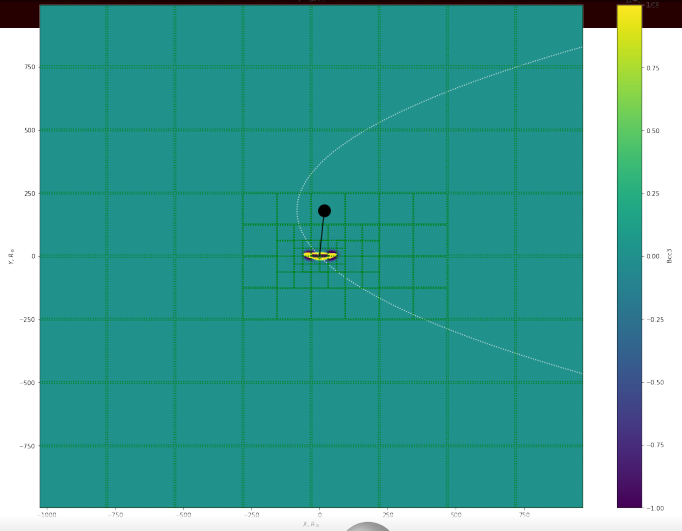
Rec3
0.75
0.50
0.25
0.00
−0.25
−0.50
−0.75
−1.00
750
500
250
0
−250
−500
−750
−1000
−750
−500
−250
0
250
500
750

Disruption timeline

- $t \simeq -1.8$**d start**
- $t = 0$ pericentre
- $t \sim 30$d fallback stream formation
- $t \sim 40 - 200$d nozzle shock
- $t \sim 50 - 250$d abalone
- $t \gtrsim 300$d thick disc stage

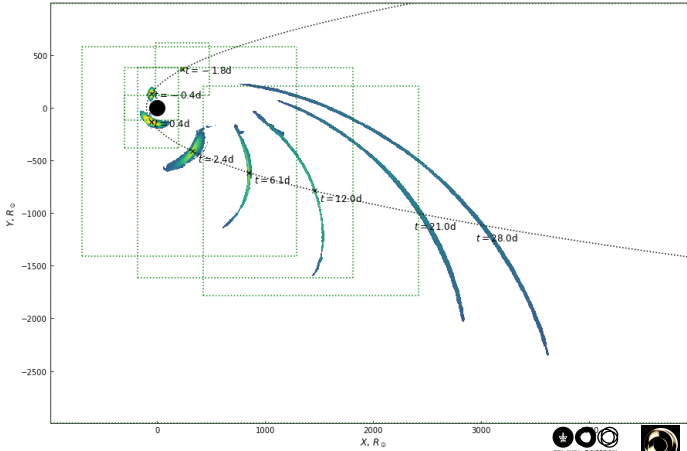

Disruption timeline

- $t \simeq -1.8$d start
- $t = 0$ **pericentre**
- $t \sim 30$d fallback stream formation
- $t \sim 40 - 200$d nozzle shock
- $t \sim 50 - 250$d abalone
- $t \gtrsim 300$d thick disc stage

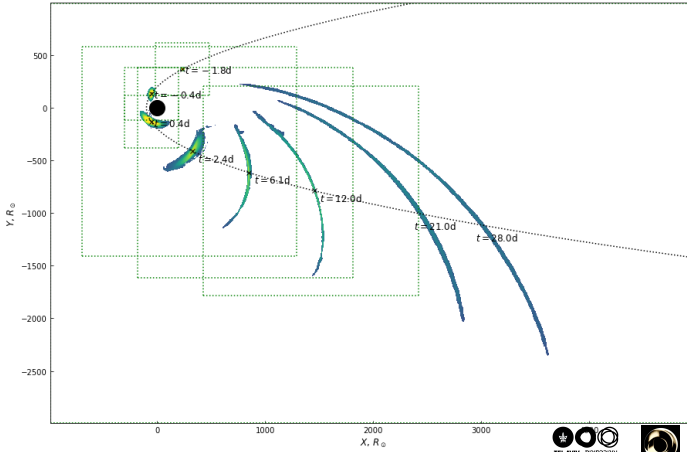

Disruption timeline

- $t \simeq -1.8$d start
- $t = 0$ pericentre
- $t \sim 30$**d fallback stream formation**
- $t \sim 40 - 200$d nozzle shock
- $t \sim 50 - 250$d abalone
- $t \gtrsim 300$d thick disc stage

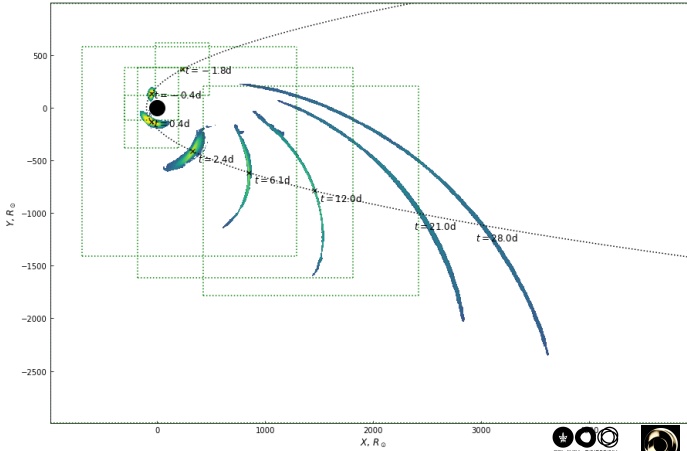

Disruption timeline

- $t \simeq -1.8$d start
- $t = 0$ pericentre
- $t \sim 30$d fallback stream formation
- $t \sim 40 - 200$**d nozzle shock**
- $t \sim 50 - 250$d abalone
- $t \gtrsim 300$d thick disc stage

Abalone (kind of a seashell):

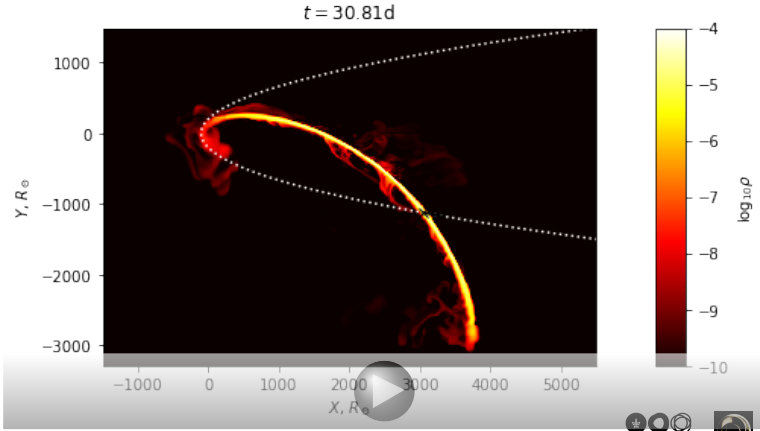

Disruption timeline

- $t \simeq -1.8$d start
- $t = 0$ pericentre
- $t \sim 30$d fallback stream formation
- $t \sim 40 - 200$d nozzle shock
- $t \sim 50 - 250$**d abalone**
- $t \gtrsim 300$d thick disc stage

pressure logarithm map:

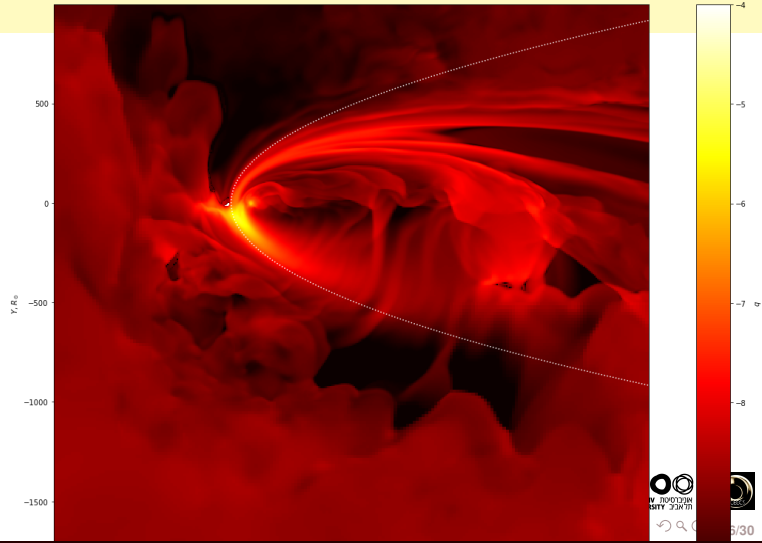

Disruption timeline

- $t \simeq -1.8$d start
- $t = 0$ pericentre
- $t \sim 30$d fallback stream formation
- $t \sim 40 - 200$d nozzle shock
- $t \sim 50 - 250$d abalone
- $t \gtrsim 300$**d thick disc stage**

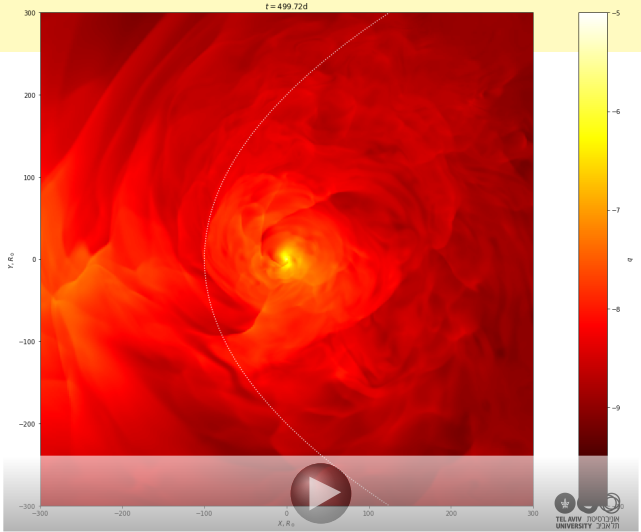

Pavel Abolmasov, Omer Bromberg, Amir Levinson, Ehud Nakar TAU/SCEECS

Nozzle shock

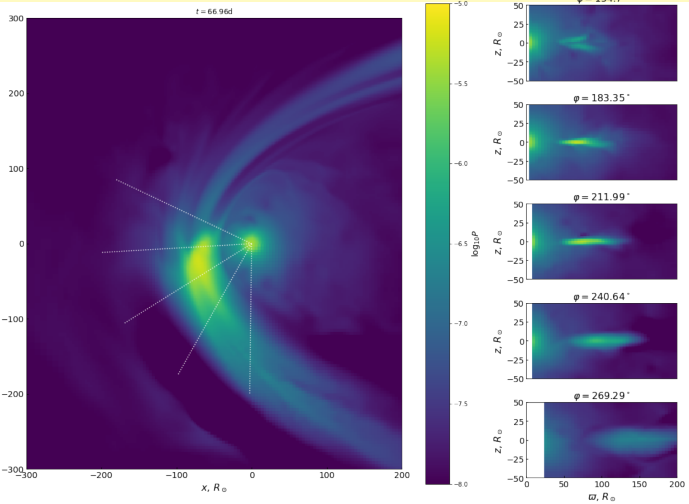

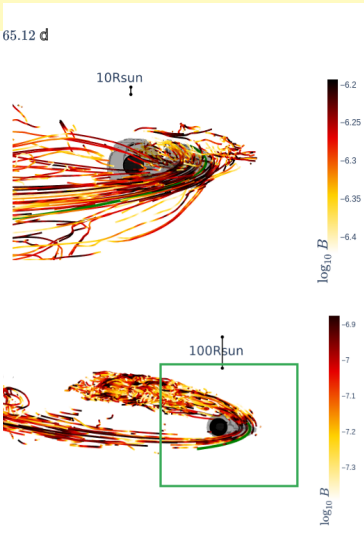

Magnetic fields in the equatorial plane

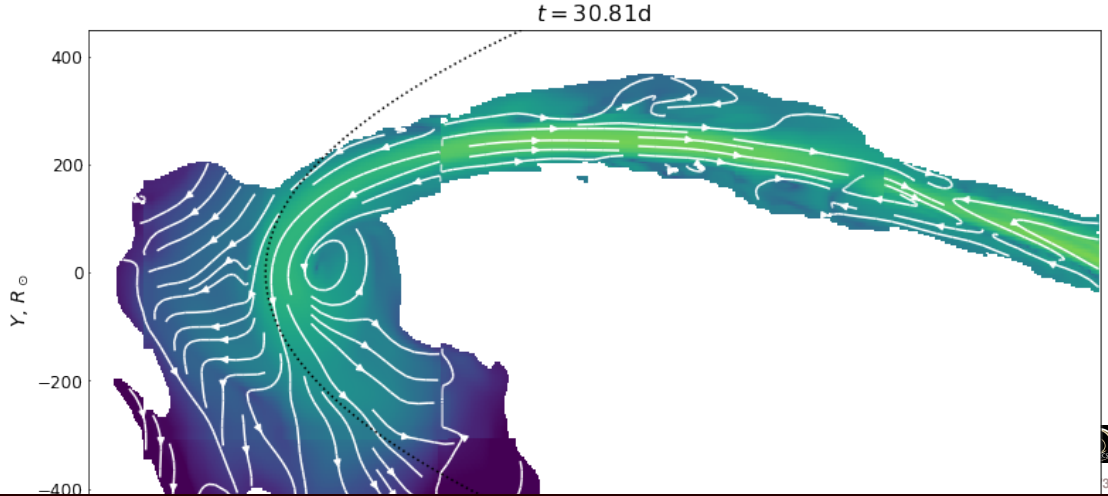

Magnetic fields in 3D

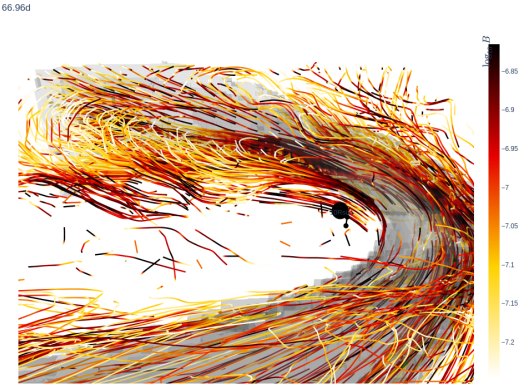

3D-rendering of magnetic field lines at $t \simeq 70$d

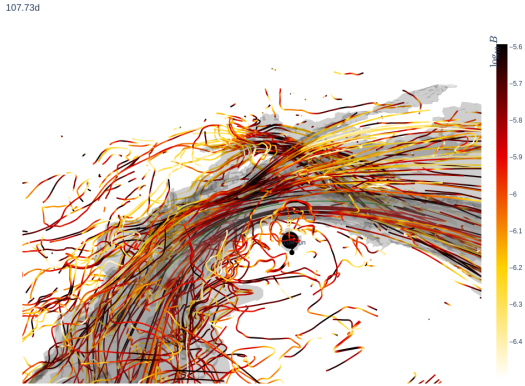

3D-rendering of magnetic field lines at $t \simeq 110$d

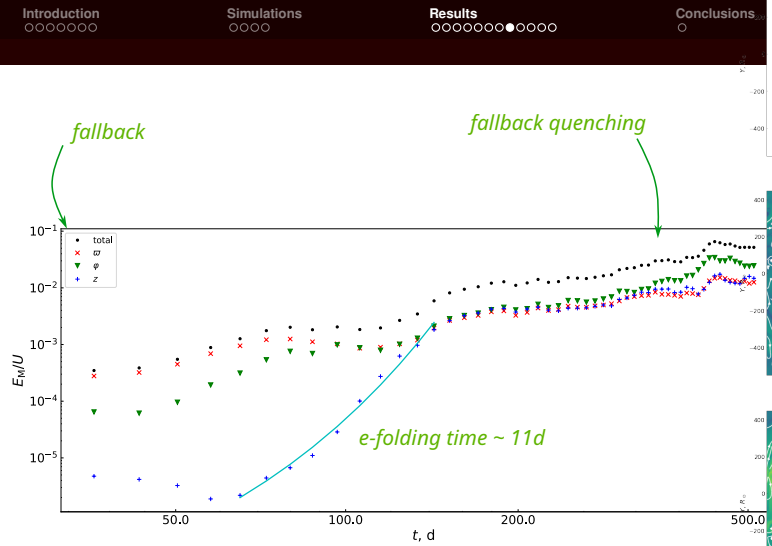

Total magnetic energy normalized by internal energy

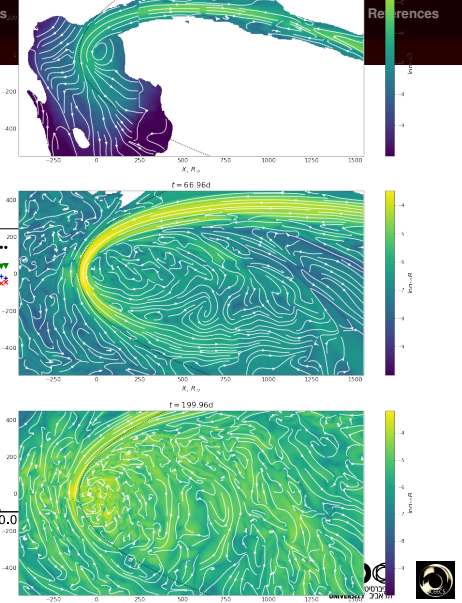

Vertical magnetic flux

One-sided flux:

$$\Phi_{\rm M} = \int_{z=0} \max(B_z, 0)\, {\rm d}x\, {\rm d}y.$$

Initial magnetic flux of a magnetized star $\sim 10^{22}$Mx

Magnetic flux required for a qualitatively different accretion regime (magnetically arrested disc)

$$B^2/8\pi \sim P_{\rm disc} \sim \dot{M}\Omega/4\pi H$$

$$\Phi_{\rm M,\ Edd} \simeq 2\pi R_{\rm in}^2 \sqrt{8\pi P} \simeq 2(2\pi)^{3/2} R_{\rm in} \sqrt{\frac{GM_{\rm BH}}{\varkappa}} \sim 10^{23} \left(\frac{M_{\rm BH}}{10^3\ {\rm M}_\odot}\right)^{3/2} {\rm Mx}.$$

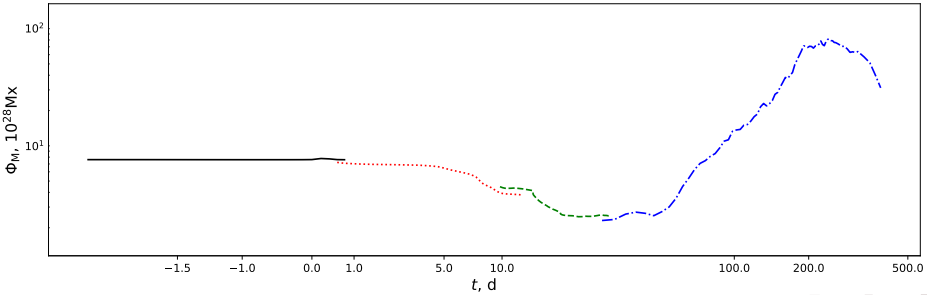

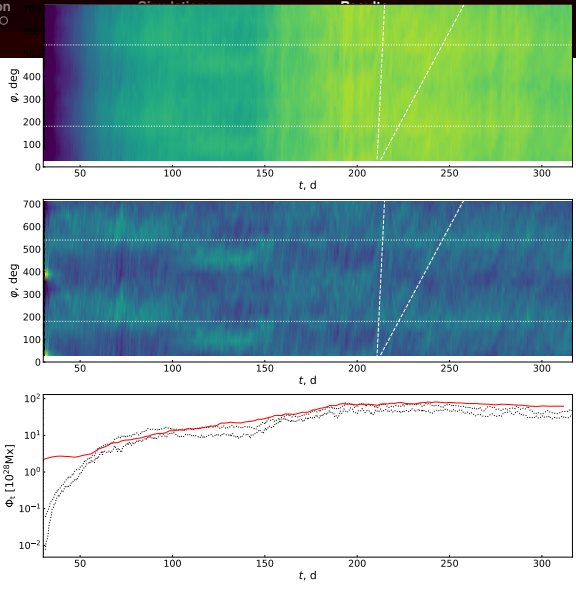

Toroidal magnetic flux:

$$\Phi_t = \int_{\varphi=\text{const},\ \varpi<\varpi_{\max}} \max(B_\varphi, 0)\,\mathrm{d}z\mathrm{d}\varpi.$$

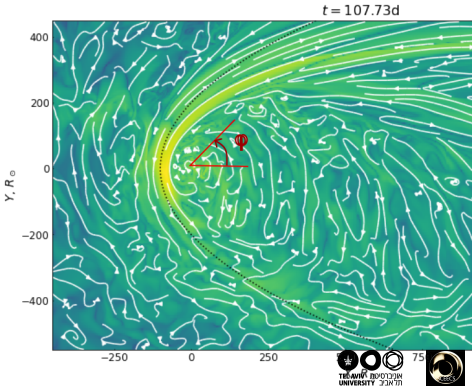

Φ_z shown in red, min and max Φ_t in black

Pavel Abolmasov, Omer Bromberg, Amir Levinson, Ehud Nakar TAU/SCEECS

Quasi-steady-state field in the disc

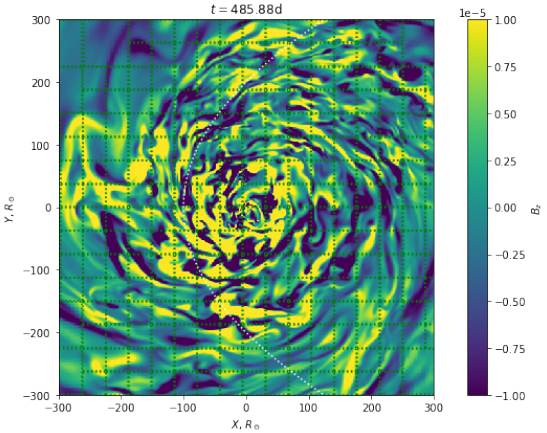

B_z map

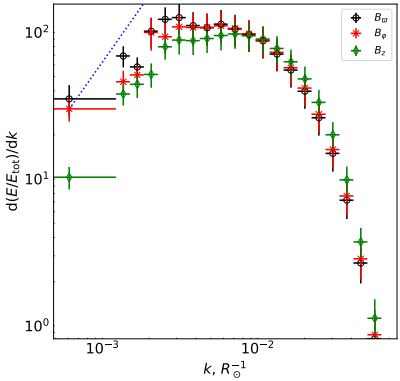

normalized PDS for B_z

PDSs for B and v components in our simulations:

Turbulent dynamo?

PDSs for MHD turbulence

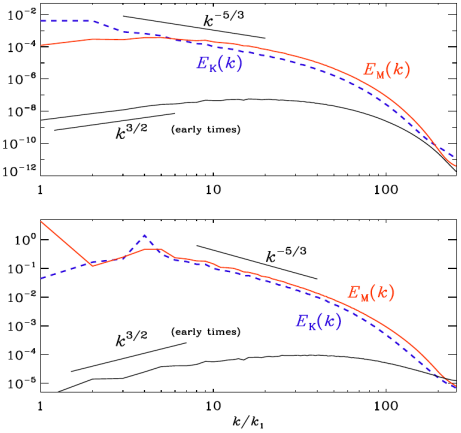

Brandenburg et al.2012)

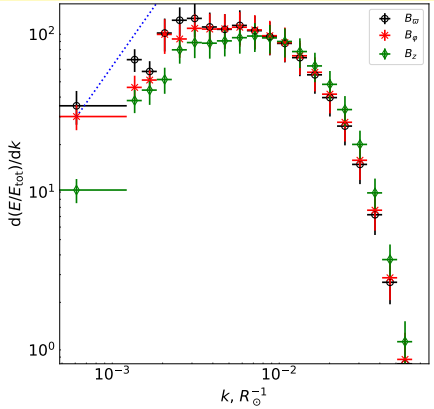

$PDS \propto k^{3/2}$ – Kazantsev's scaling (Kazantsev1968)

Summary

1. Slow circularization by turbulent motions
2. Vertical magnetic field generation and overall amplification associated with the nozzle shock
3. Fields amplified up to equipartition ($\beta \sim 10 - 100$)
4. Chaotic fields in the disc with a typical scale $\lesssim 0.5 R_{\rm p}$

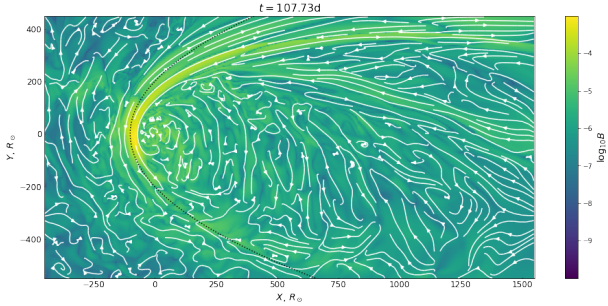

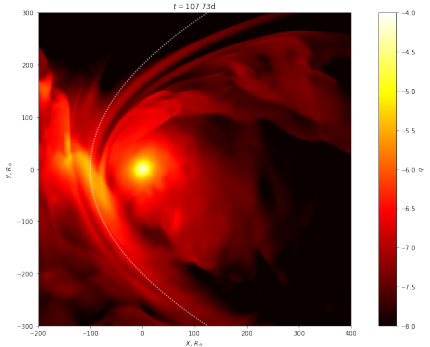

Thank you for attention!

Triangular plot

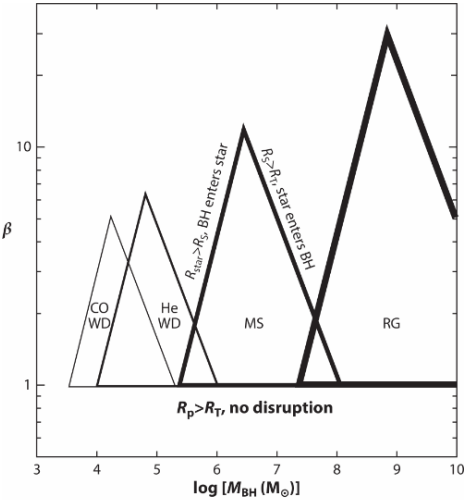

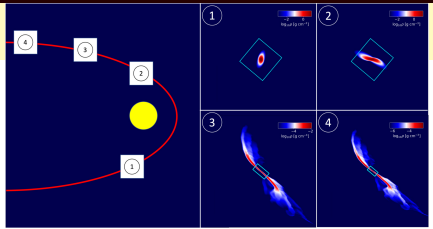

Ryu et al.2023), $M_{\rm BH} = 10^5\ {\rm M}_\odot$

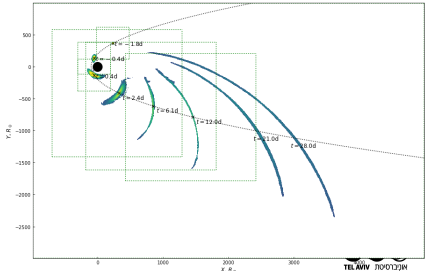

this work, $M_{\rm BH} = 10^5\ {\rm M}_\odot$

Circularization

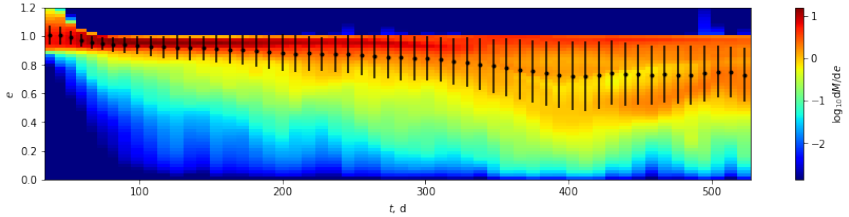

eccentricity distribution as a function of time

$$e = \sqrt{1 + \frac{2\varepsilon l^2}{G^2 M_{\rm BH}^2}},$$

where

$$l = |\mathbf{r} \times \mathbf{v}|,$$

$$\varepsilon = v^2/2$$

(see for example Andalman et al.2022)

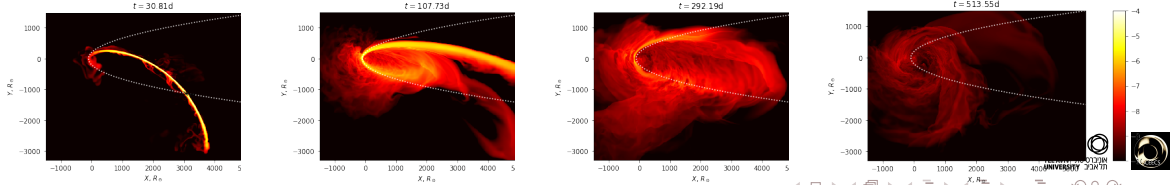

Resolution effects

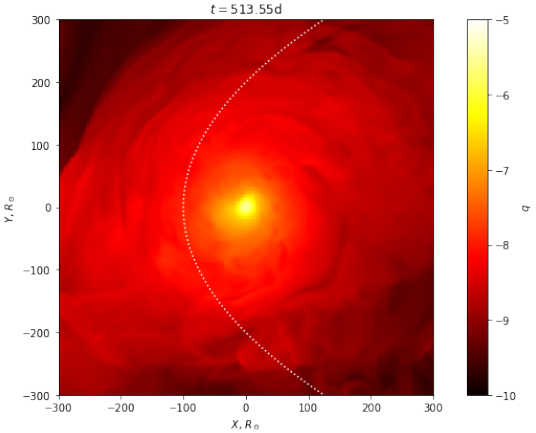

low-res (2 $R_\odot$) + 10 $R_\odot$ smoothing radius for the BH potential

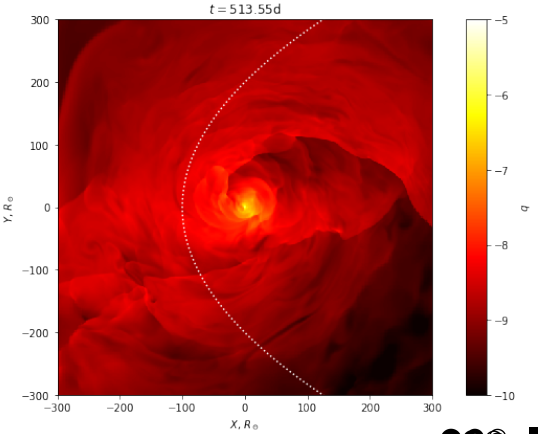

high-res (1 $R_\odot$) + 1 $R_\odot$ smoothing radius for the BH potential

Thick disc ($t = 500 - 550$d)

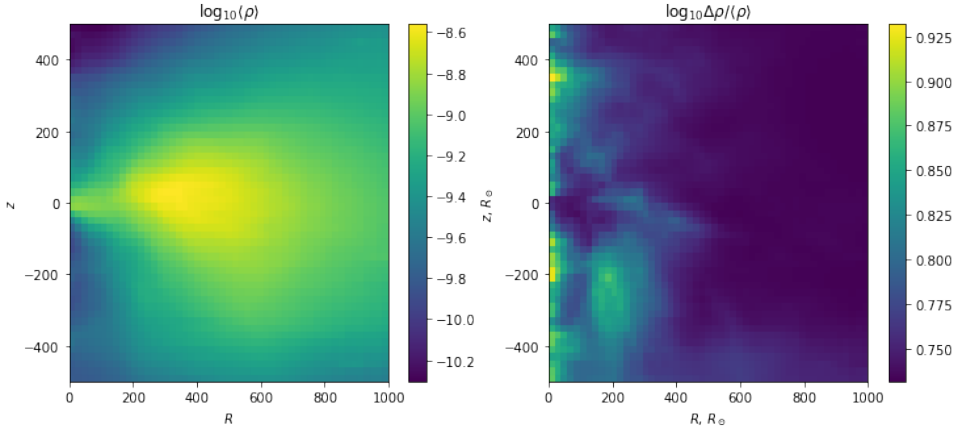

density (averaged over 30 frames and azimuth, `BHz`)

Thick disc ($t = 500 - 550$d): magnetic field tensions

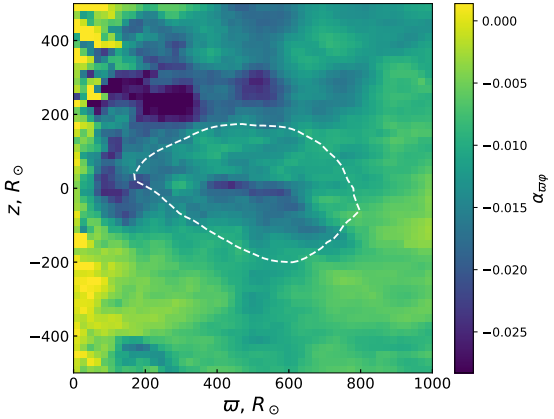

effective magnetic viscosity parameter $\alpha \sim 0.02$ (Shakura & Sunyaev1973)

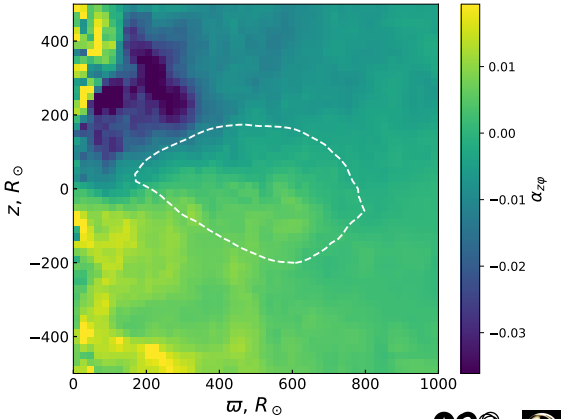

angular momentum transported away from the disc

Pavel Abolmasov, Omer Bromberg, Amir Levinson, Ehud Nakar TAU/SCEECS

Andalman Z. L., Liska M. T. P., Tchekhovskoy A., Coughlin E. R., Stone N., 2022, MNRAS, 510, 1627

Brandenburg A., Sokoloff D., Subramanian K., 2012, SSR, 169, 123

Cendes Y., et al., 2024, ApJ, 971, 185

Coughlin E. R., Nixon C., Begelman M. C., Armitage P. J., Price D. J., 2016, MNRAS, 455, 3612

Dai L., McKinney J. C., Miller M. C., 2015, ApJL, 812, L39

Evans C. R., Kochanek C. S., 1989, ApJL, 346, L13

Gezari S., 2021, ARA&A, 59, 21

Goodwin A. J., et al., 2025, ApJSS, 278, 36

Guillochon J., McCourt M., 2017, ApJL, 834, L19

Guillochon J., Ramirez-Ruiz E., 2013, ApJ, 767, 25

Hills J. G., 1975, Nature, 254, 295

Kazantsev A. P., 1968, Soviet Journal of Experimental and Theoretical Physics, 26, 1031

Lidskii V. V., Ozernoi L. M., 1979, Soviet Astronomy Letters, 5, 16

Liodakis I., et al., 2023, Science, 380, 656

Mainetti D., Lupi A., Campana S., Colpi M., Coughlin E. R., Guillochon J., Ramirez-Ruiz E., 2017, A&A, 600, A124

Pacuraru S., Bonnerot C., Pessah M. E., 2026, MNRAS, 548, stag603

Piran T., Svirski G., Krolik J., Cheng R. M., Shiokawa H., 2015, ApJ, 806, 164

Rees M. J., 1988, Nature, 333, 523

Ryu T., Krolik J., Piran T., Noble S. C., Avara M., 2023, ApJ, 957, 12

Shakura N. I., Sunyaev R. A., 1973, A&A, 24, 337

Shu X., et al., 2020, Nature Communications, 11, 5876

Steinberg E., Stone N. C., 2024, Nature, 625, 463